



Analysis of compliant mechanisms with series and parallel substructures through the ellipse of elasticity theory

O. Sorgonà^a, S. Serafino^b, O. Giannini^a, M. Verotti^{b,*}

^a Department of Industrial Engineering, Niccolò Cusano University of Rome, Via Don Carlo Gnocchi 3, 00166 Rome, Italy

^b Department of Mechanical, Energy, Management and Transportation Engineering, University of Genova, Via all'Opera Pia, 15 - 16145 Genoa, Italy

ARTICLE INFO

Keywords:
Flexures
Ellipse of elasticity
Compliant mechanisms
Parallel substructures

ABSTRACT

Compliant mechanisms with complex hybrid configurations have been designed to meet the requirements of specific applications demanding high performance. Kinetostatic analysis, fundamental at the early stage of design, can become difficult for compliant systems characterized by series and parallel substructures. In the present paper, the ellipse of elasticity method is implemented for the analysis of a compliant mechanism with hybrid topology. Firstly, the ellipses associated to the different flexure hinges, characterized by uniform or non-uniform cross-sections, and by constant or variable initial curvature, are determined. Then, the unique ellipse representing the compliant mechanism is obtained by means of series and parallel compositions. By exploiting the antiprojective polarity properties of the ellipse, the kinetostatic analysis of the compliant system is reduced to a geometric problem with a straightforward solution. Linear and nonlinear finite element analyses and experimental tests are performed to verify the theoretical results.

1. Introduction

Compliant mechanisms, through the deflections of flexible elements, transmit force and motion avoiding wear, friction, and backlash. Because of these advantages, compliant systems have been implemented in a variety of scientific and industrial fields (Howell et al., 2013). Many applications can be found in precision engineering (Wang et al., 2021; Wu and Xu, 2018), optics (Li et al., 2017; Zhao et al., 2020), MEMS (Saito et al., 2016; Hao and Zhu, 2019), and robotics (Bilancia et al., 2021b; Morales Bieze et al., 2020). Mechanical applications include constant-force mechanisms (Wang and Xu, 2018; Bilancia and Berselli, 2020), compliant inverters (Huang et al., 2014) and amplifiers (Xu and Li, 2011), compliant joints (Li and Hao, 2022) and shells (Radaelli and Herder, 2017), grippers (Verotti et al., 2017; Ali and Shimoda, 2023), multi-stable (Santer and Pellegrino, 2008; Chen et al., 2023) and origami (Lang et al., 2018) devices.

Stiffness, range of motion, or, more in general, application-specific kinetostatic requirements (Djourachkovitch et al., 2023), led to the design of systems composed of series and/or parallel arrangements of flexible and rigid elements, often resulting in complex hybrid topologies (Chen et al., 2016; Zhu et al., 2018b). Considering also the geometric profile variety of the flexure hinges and beams (Bilancia and Berselli, 2021), the kinetostatic analysis of a compliant mechanism can become a challenging task. To deal with this issue, many strategies have been proposed for the solution of problems characterized by

linear deflections or geometric nonlinearities (Cammarata et al., 2016; Bilancia et al., 2021a; Cao et al., 2023).

In the following, the methods proposed for the small deflections case are briefly recalled, whereas insights on large deflections analysis, such as elliptic integral solutions (Zhang and Chen, 2013; Cammarata et al., 2018), pseudo-rigid body models (Jin et al., 2020), or beam constraint models (Awtar et al., 2006; Awtar and Sen, 2010; Chen et al., 2019), can be found in Hao et al. (2016).

Finite element analysis has been performed for a variety of complex-topology mechanisms (Friedrich et al., 2014). However, its implementation could be time-consuming and results depend on the number of elements (Donaldson, 2008). Elastic beam theory has been extensively applied for the analysis of compliant systems, as mechanical amplifiers (Ling et al., 2016) and parallel guiding mechanisms (Luo et al., 2015). However, the elastic line solution can become complicated for several geometries, loads, or boundary conditions (Shooshtari and Khajavi, 2010; Balduzzi et al., 2016). Castigliano's theorems have been used effectively in the analysis of non-uniform flexures (Lobontiu et al., 2002, 2000) and of different compliant systems, as grasping (Kurita et al., 2012; Chen et al., 2016), nanopositioning (Kenton and Leang, 2012; Yong and Mohemani, 2013), and amplification (Ueda et al., 2010; Schultz and Ueda, 2013) mechanisms. Even though analytical formulations can be obtained, the solution of the energy equations can

* Corresponding author.

E-mail address: matteo.verotti@unige.it (M. Verotti).

get difficult in case of complex geometries or configurations (Ling et al., 2020). The virtual work principle has been also used to determine the compliance models of various flexures (Chen et al., 2009; Li et al., 2013).

The compliance matrix method, not requiring the calculus of the internal forces, proved to be suitable for the analysis of compliant mechanisms with series and parallel topologies (Su et al., 2012; Lobontiu, 2014), such as micro positioning stages (Qu et al., 2016) and displacement amplifiers (Dong et al., 2018). In this approach, flexures are modeled as kinetostatic functions arranged according to network principles. However, the modeling procedure becomes complicated in case of multiple applied forces (Ling et al., 2020; Arredondo-Soto et al., 2022) and the complete displacements evaluation needs further kinematic analyses (Zhu et al., 2018a).

A semi-analytical matrix displacement approach, based on the matrix displacement and on the transfer matrix methods, has been proposed for the modeling of compliant mechanisms with serial-parallel substructures (Ling et al., 2018). The method implementation requires the solution of the equilibrium equations at the nodes.

To avoid the solution of the equilibrium equations, an energy approach based on the screw theory was presented in Wu et al. (2019). However, due to the large number of elements, a condensed approach was further presented, based on energy conservation law, equilibrium equations of nodal forces, and transfer matrix approach (Wu et al., 2022).

Regarding the geometrical interpretation of compliance, the center of elasticity and force-compliant axes were introduced in Lipkin and Patterson (1992a,b). In case of planar deflections, the center of elasticity has been considered to develop an intrinsic geometrical framework based on two conic sections, that are the single-point compliance ellipse and the single-point stiffness ellipse. These ellipses require the definition of two associated coupling vectors, also depending on the choice of a reference point (Krishnan et al., 2010).

Recently, the ellipse of elasticity theory was applied to the kinetostatic analysis of the compliant mechanisms (Sorgonà et al., 2023). With respect to the geometrical framework presented in Krishnan et al. (2010), this model is based on a unique conic section called *ellipse of elasticity*. The ellipse of elasticity associated to an elastic suspension represents the antiprojective polarity transformation between poles of displacements and lines of action of forces that cause the deflection. Therefore, it is not limited to the single-point condition.

The main advantage of the ellipse of elasticity approach consists of transforming the deflection analysis, which is generally an analytical or a numerical problem, into a *geometric* problem. Furthermore, in addition of reducing to one the number of the involved geometric entities, the model no longer needs a reference point to be chosen.

More specifically, the first step of the method consists of determining the ellipse of elasticity corresponding to each flexure of the compliant mechanism. By resorting to the geometry of masses theory, this step can be readily performed for complex flexible elements, even if characterized by variable curvature, variable cross-section, or, more in general, variable flexural rigidity. The second step consists of the reduction of the ellipses by series and parallel compositions. Solutions of balance or energy equations are not required, because static balance and geometric congruence are implicitly taken into account in the compositions.

The procedure leads to the definition of a unique ellipse not dependent on the load conditions. This conic defines, for every applied load, the position of the pole of the displacements of the end-effector link with respect to the frame link. This relation is accomplished through a straightforward geometric procedure.

These features make this approach suitable and particularly advantageous in case of complex-topology mechanisms with multiple serial and parallel substructures. Since each substructure is systematically reduced, the ellipses' composition leads to a geometric representation

of the whole compliant mechanism as a two-port system. This condensed model embeds completely the input/output force-displacement relations.

In this paper, the ellipse of elasticity method, previously applied to a basic-topology mechanism, is fully exploited for the straightforward analysis of a hybrid compliant mechanism, characterized by series and parallel substructures. More specifically, a compliant mechanism composed of two closed chains and one open chain is considered. The elastic elements of the substructures have different geometric layouts, with uniform or non-uniform cross-section, and axis with various curvature. In particular, a flexure with parabolic axis is introduced and its corresponding ellipse is defined resorting to closed-form solutions. Linear and nonlinear finite element simulations and an experimental campaign are carried out to verify the theoretical results and to validate the implemented procedure.

2. Problem statement

To facilitate the synthesis or the analysis procedures, a compliant mechanism can be generally associated to a pseudo-rigid body model (PRBM), according to the rigid-body replacement method (Howell et al., 2013). In turn, a rigid-body mechanism can be represented by its corresponding graph, according to graph theory (Tsai, 2000). Fig. 1 shows a generic compliant mechanism (a), its corresponding PRBM (b), and the graph representation of the PRBM (c).

PRBMs can be composed of arrangements of open and closed kinematic chains, resulting in complex hybrid topologies. In these cases, the kinetostatic analysis of the corresponding compliant mechanism can become challenging. However, if the PRBM can be represented by a series-parallel graph (Bodirsky et al., 2007), the ellipse of elasticity theory can be implemented to transform the analysis into a geometrical problem with a straightforward solution. According to this theory, each flexible element can be associated to an ellipse of elasticity that represents its kinetostatic behavior. Then, the ellipses can be composed, through series and parallel reductions, into a unique ellipse that represents the compliant mechanism as one elastic suspension connecting the end-effector link to the frame link.

Once this ellipse is determined, the kinetostatic analysis can be performed by exploiting the antiprojective polarity properties of ellipses.

3. Theoretical background

Every elastic suspension connecting two rigid bodies, composed of a single element or of a complex arrangement of flexible and rigid elements, can be represented by a geometric entity called *ellipse of elasticity* (Culmann, 1875; Ritter, 1888). With reference to Fig. 2, the application of a force \mathbf{R}_i or \mathbf{R}_j to the bodies i or j , respectively, determines the deformation of the suspension e_{ji} and a consequent relative displacement of the rigid bodies. The ellipse of elasticity \mathcal{E}_{ji} , with center C , establishes a bijective correspondence between the line of action p of the applied force and the resulting pole of displacements P_{ji} . More specifically, this correspondence is defined as *antiprojective polarity transformation* between antipolars, which are the lines of action, and antipoles, which are the poles of displacements. Since this transformation is defined in the projective plane $\mathbb{P}\mathbb{R}^2$, the correspondence holds also for the points at infinity and the line at infinity. As a consequence, pure translations and pure moments can be considered in the transformation.

3.1. Antiprojective polarity

The fundamental properties of the antiprojective polarity transformation are represented in 3. Different cases can be considered depending on the position of the line of action with respect to the ellipse.

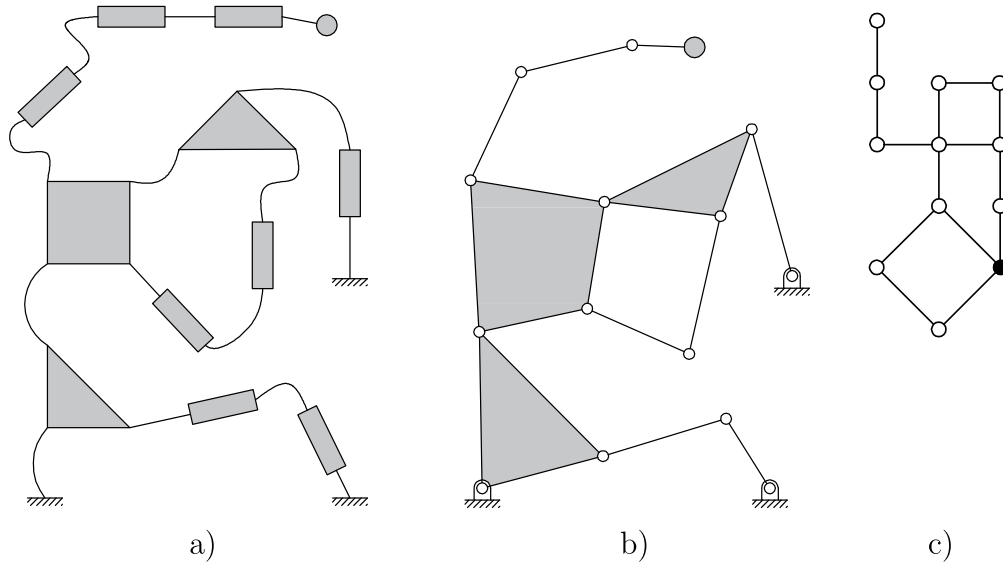


Fig. 1. Hybrid compliant mechanism (a), PRBM (b), and graph (c).

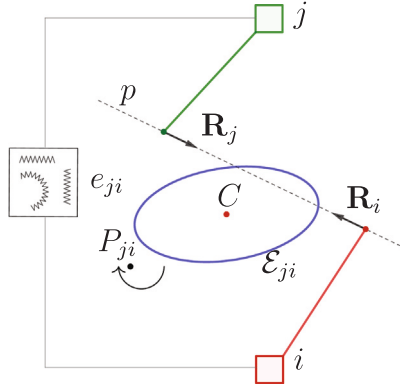


Fig. 2. Ellipse of elasticity \mathcal{E}_{ji} associated to the elastic suspension e_{ji} connecting the rigid bodies i and j , line of action p and pole of displacements P_{ji} .

- (a) The corresponding antipole P_c of a line of action p_c , passing through the center C of ellipse, lies at infinity. Therefore, the relative displacement of the rigid bodies is a pure translation (Fig. 3(a)). The line p_c is defined as a diameter of the ellipse;
- (b) the corresponding antipole P_s of a secant line of action p_s lies outside of the ellipse (Fig. 3(b));
- (c) the corresponding antipole P_t of a tangent line of action p_t lies on the ellipse and it is the symmetric of the tangent point Fig. 3(c);
- (d) the corresponding antipole P_e of an exterior line of action, p_e , lies inside the ellipse (Fig. 3(d));
- (e) the corresponding antipole of the line of action at infinity, p_∞ , is the ellipse center C (Fig. 3(e)). Therefore, the application of a pure moment determines a rotation about the ellipse center.

In the previous cases, parallel lines of action have been considered. Because of the antiprojective polarity properties, the antipoles of parallel lines of action lie on the same line q_c , that is a diameter of the ellipse. The generic line of action p , with antipole P , intersects q_c in P' determined as

$$\overline{CP} \overline{CP'} = \overline{CP_t}^2 \quad (1)$$

The diameters p_c and q_c define a pair of *conjugate* diameters. It is worth noting that every two ellipses have at least one pair of conjugate diameters in common (Glaeser et al., 2016). In fact, with reference to

Fig. 3(f), the two concentric non-similar ellipses intersect in the points A , B , C , and D , which define a parallelogram. The common conjugate diameters p_c and q_c are parallel to the sides BC , AD , and to the sides AB , CD , respectively. If the ellipses are similar, any pair of conjugate diameters is common.

3.2. Kinetostatic modeling

The compliance behavior of the elastic suspension is represented by the *elastic weight* w , defined through the relation

$$\theta = w M \quad (2)$$

where θ is the relative rotation of the bodies and M is the moment evaluated at the center of the ellipse. The elastic weight determines also the translational compliances of the suspension. In fact, it can be demonstrated that

$$\lambda_a = w b^2, \quad \lambda_b = w a^2 \quad (3)$$

where λ_a and λ_b represent the translation compliances along the directions of the ellipse axes.

The detailed evaluation of the geometric and elastostatic parameters of the ellipse, that are the position of its center C , the orientation α and the lengths of its semi-axes a and b , and the elastic weight w , is reported in Section 3.3.

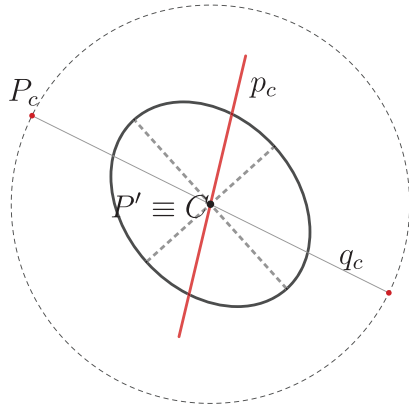
3.3. Determination of the ellipse of elasticity

The ellipse of elasticity of the generic flexure, modeled as an elastic beam with variable curvature and variable cross-section, corresponds to the central ellipse of inertia of its compliance distribution (Sorgonà et al., 2023). As a consequence, the procedure for determining the ellipse of elasticity is analogous to the determination of the ellipse of inertia, on the condition that the mass distribution of the element is substituted by its compliance distribution.

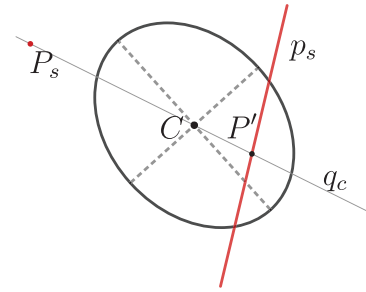
A generic initially-curved flexure, fixed at the origin of the reference frame $\{Oxy\}$ having axis length l , is shown in Fig. 4. The elastic line is described by means of the arc-length coordinate system with arc-length parameter $s \in [0, l]$.

The compliance distribution $c(s)$ can be written as

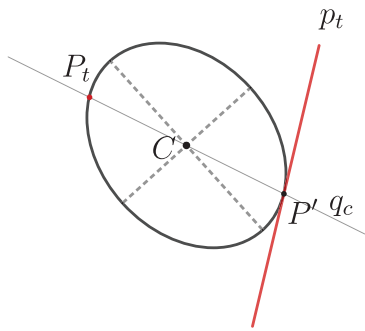
$$c(s) = \frac{1}{E(s)I(s)} \quad (4)$$



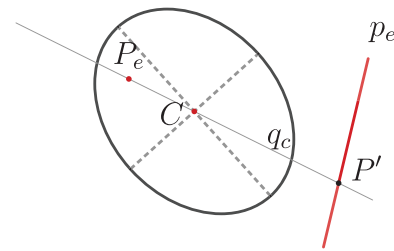
(a) Antipole of a diameter



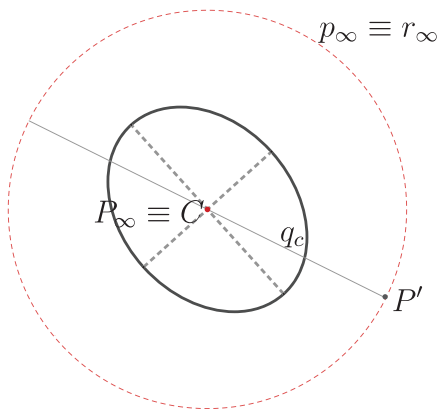
(b) Antipole of a secant line



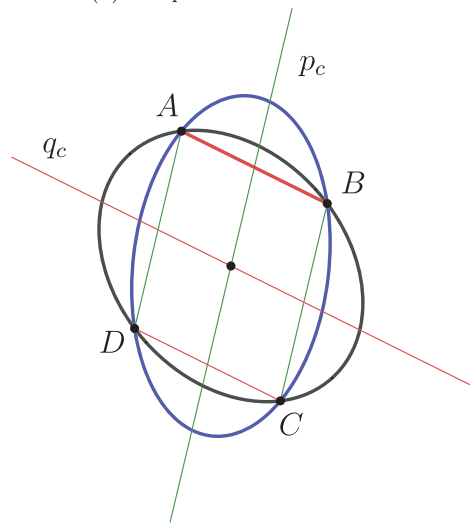
(c) Antipole of a tangent line



(d) Antipole of an exterior line



(e) Antipole of the improper line



(f) Common conjugate diameters of two ellipses.

Fig. 3. Properties of the antiprojective polarity transformation.

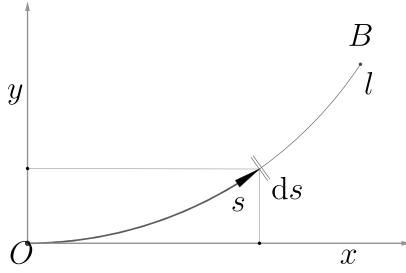


Fig. 4. Flexure nomenclature.

where $E(s)$ is the Young's modulus and $I(s)$ is the moment of inertia of the cross-section with respect to the bending axis. Following the geometry of masses theory, the elastic weight is given by

$$w = \int_0^l c(s)ds, \quad (5)$$

that is the zeroth-order moment of the distribution $c(s)$. The position of the barycenter C of the distribution can be obtained as

$$x_c = \frac{S_x}{w}, \quad y_c = \frac{S_y}{w}, \quad (6)$$

where S_x and S_y are the first-order moments of the distribution. In particular, the point $C \equiv (x_c, y_c)$ is the center of the ellipse of elasticity.

The second-order moments of the compliance distribution can be calculated with respect to a central reference frame $\{C x_0 y_0\}$, with origin in C and axis x_0 and y_0 parallel to x and y , respectively. These moments can be arranged in a 2×2 symmetric matrix as

$$S_0 = \begin{bmatrix} S_{x_0 x_0} & -S_{x_0 y_0} \\ -S_{x_0 y_0} & S_{y_0 y_0} \end{bmatrix}. \quad (7)$$

The matrix S_0 can be calculated also in the principal reference frame $\{C \xi \eta\}$, rotated of the angle

$$\alpha = \frac{1}{2} \arctan \frac{2S_{x_0 y_0}}{S_{y_0 y_0} - S_{x_0 x_0}} \quad (8)$$

with respect to the frame $\{C x_0 y_0\}$. In this case, the central second-order moments matrix becomes

$$S_\alpha = \begin{bmatrix} S_{\xi\xi} & 0 \\ 0 & S_{\eta\eta} \end{bmatrix}, \quad (9)$$

where $S_{\xi\xi}$ and $S_{\eta\eta}$ are *principal* second-order moments, i.e. moments with minimum and maximum values with respect to α , respectively.

The angle α defines the orientation of the ellipse semi-axes, whose lengths, according to Eq. (3), can be expressed as

$$a = \sqrt{\frac{S_{\eta\eta}}{w}}, \quad b = \sqrt{\frac{S_{\xi\xi}}{w}}. \quad (10)$$

The geometric parameters x_c , y_c , α , a , b , and the elastostatic parameter w , completely define the ellipse of elasticity of the elastic element.

3.4. Series and parallel compositions of the ellipses of elasticity

Figs. 5(a) and 5(b) show the ellipses of elasticity \mathcal{E}_1 and \mathcal{E}_2 associated to the elastic elements e_1 and e_2 , respectively. In the case of a series arrangement, the elastic elements connect the rigid bodies i , k , and j , as depicted in Fig. 5(c). In the case of a parallel arrangement, the elastic elements connect i and j , as depicted in Fig. 5(d). Each figure depicts also the resultant ellipses, which are \mathcal{E}_Σ and \mathcal{E}_Π , for the series and parallel arrangement, respectively. The ellipses are defined according to the procedure reported in Sorgonà et al. (2023), that can be summarized by the relations listed in Tables 1 and 2.

Table 1
Definition of the ellipses corresponding to the series composition.

0th	$w_\Sigma = w_1 + w_2$
1st	$w_1 \overline{C_1 \Sigma} = w_2 \overline{C_2 \Sigma}$
2nd	$S_{0,\Sigma} = S_{0,1} + S_{0,2} + \begin{bmatrix} 0 & 0 \\ 0 & w_1 \overline{C_1 \Sigma}^2 + w_2 \overline{C_2 \Sigma}^2 \end{bmatrix}$

Table 2
Definition of the ellipses corresponding to the parallel composition.

0th	$\frac{1}{w_\Pi} = \frac{1}{w_1} \left(1 + \frac{C_1 P_1^2}{d_{q1}^2} + \frac{C_1 Q_1^2}{d_{q1}^2} \right) + \frac{1}{w_2} \left(1 + \frac{C_2 P_2^2}{d_{q2}^2} + \frac{C_2 Q_2^2}{d_{q2}^2} \right)$
1st	$\frac{1}{w_1 d_{q1}^2} \overline{C_1 Q_1} = \frac{1}{w_2 d_{q2}^2} \overline{C_2 Q_2}, \quad \frac{1}{w_1 d_{q1}^2} \overline{C_1 P_1} = \frac{1}{w_2 d_{q2}^2} \overline{C_2 P_2}$
2nd	$S_{0,\Pi}^{-1} = \begin{bmatrix} k_a \cot^2 \widehat{pq} + \frac{k_b}{\sin^2 \widehat{pq}} & k_a \cot \widehat{pq} \\ k_a \cot \widehat{pq} & k_a \end{bmatrix} (*)$
(*)	$k_a = \left(\frac{1}{w_1 d_{q1}^2} + \frac{1}{w_2 d_{q2}^2} \right), \quad k_b = \left(\frac{1}{w_1 d_{q1}^2} + \frac{1}{w_2 d_{q2}^2} \right)$

4. Design of the hybrid compliant mechanism

The rigid-body mechanism serving as pseudo-rigid body model is depicted in Fig. 6. From a kinematic point of view, the mechanism is composed of two closed chains defining a six-bar Stephenson mechanism, and of a two-link open chain.

The corresponding compliant mechanism, obtained by applying the rigid-body replacement method, is shown in Fig. 7. The revolute joints of the rigid-body mechanism are substituted with different flexures, according to the following scheme:

- joints A are replaced by uniform, constant-curvature flexures. More specifically, flexures $A_1 - A_4$ have radius $r = 13.33$ mm and subtend the angle $2\phi = 50^\circ$, whereas A_5 is a straight-axis flexure with axis length $l = 9.00$ mm;
- joints B are replaced by uniform parabolic-axis flexures with axis equation $y = 0.075x^2$, with $x \in [4.00, 15.80]$ mm;
- joints C are replaced by non-uniform straight-axis flexures. More specifically, the variable cross-section delineates two circular profiles, symmetric with respect to the flexure axis, with equation $h(x) = h_0 + 2(R - \sqrt{R^2 + x^2})$, with $x \in [-8.00, 8.00]$ mm, $h_0 = 2.00$ mm, and $R = 132.83$ mm.

The in-plane thickness of flexures A and B is $h = 1$ mm, and the out-of-plane thickness, equal for all the flexures, is $b = 10$ mm. The pose of the flexures is defined by the data listed in Table 3, considering the reference frame $\{Oxy\}$ introduced in Fig. 7. A homogeneous and isotropic material is considered for the theoretical analysis. A Young's modulus $E = 2945$ MPa is imposed, according to the material properties of the prototype fabricated for the experimental campaign, as described in Section 7.

5. Application of the ellipse of elasticity theory

To perform the kinetostatic analysis of the compliant mechanism, the ellipses of the elasticity of each flexure must be firstly determined. Then, the ellipse associated to the whole mechanism can be evaluated as a composition of the previous ones.

5.1. Ellipses of elasticity of the single flexures

The flexible elements used in the rigid-body replacement step are depicted in Table 4. For each element, the table lists the geometric parameters and the relations used to define the corresponding ellipse, according to the procedure described in Section 3.3. Further details

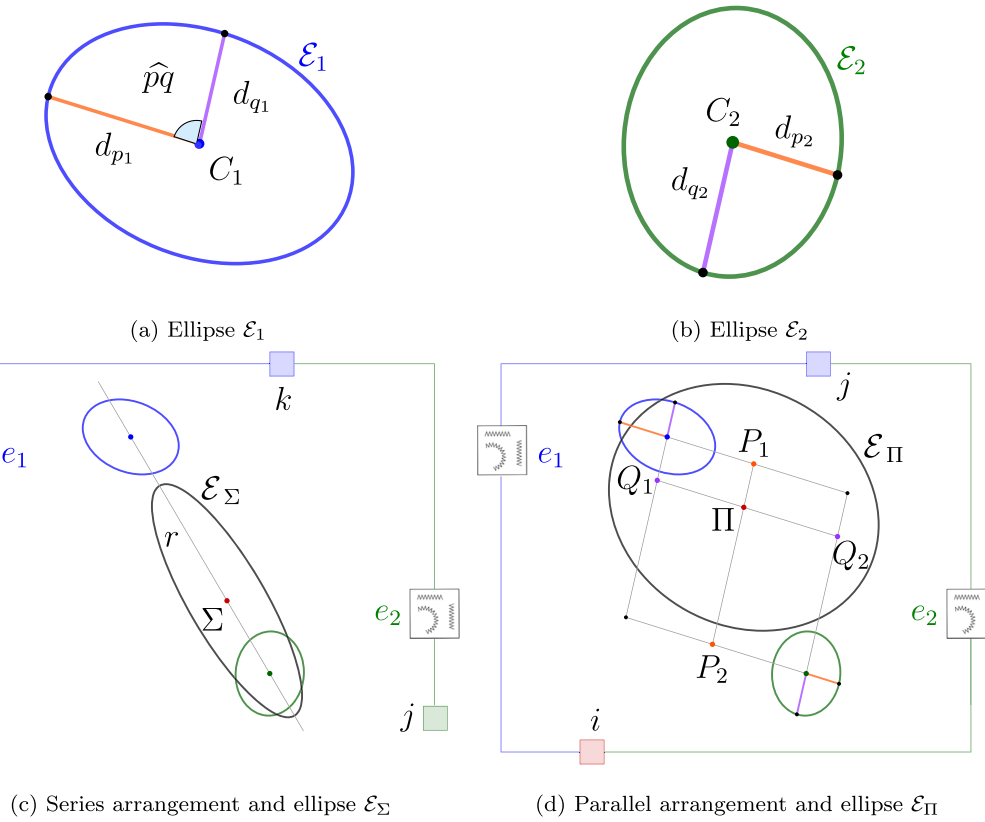


Fig. 5. Definition of the ellipses corresponding to the series and parallel composition.

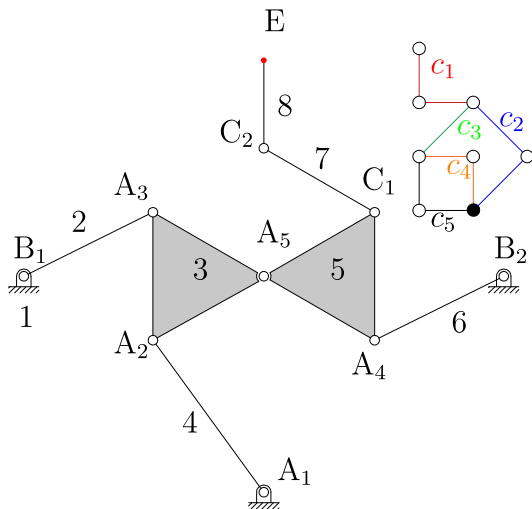


Fig. 6. Hybrid rigid-body mechanism.

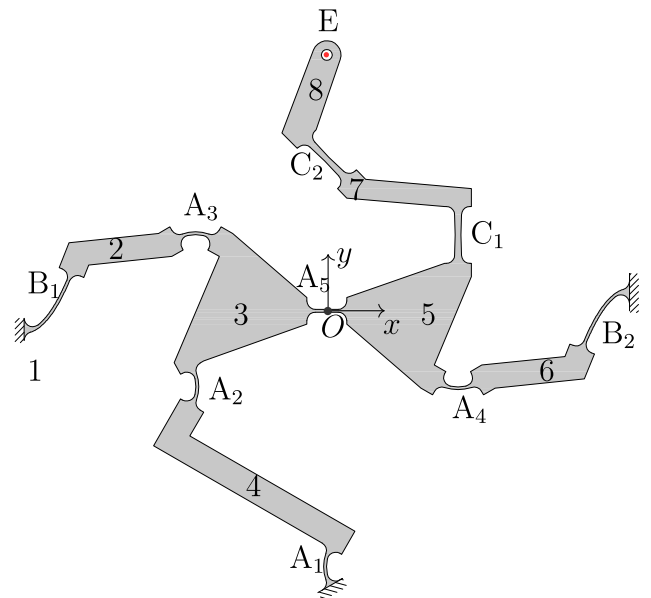


Fig. 7. Hybrid compliant mechanism.

regarding the uniform flexure with straight and parabolic axis are reported in Appendix A and Appendix B, respectively.

The determined ellipses are shown in Fig. 8, whereas the numerical values of center coordinates, semi-axes lengths, orientations, and elastic weights, are listed in Table 5.

5.2. Ellipse of elasticity of the compliant mechanism

The ellipse of elasticity associated to the hybrid compliant mechanism can be defined by implementing a set of series and parallel

compositions. Each composition results in a kinetostatic equivalent compliant system with simplified topology.

With reference to Figs. 6 and 7, the end-effector link 8 is connected to the frame 1 by means of several open and closed chains. The first open chain, c_1 , is composed of bodies 8,7, 5 and flexures C_2 and C_1 . Body 5 is connected to the frame 1 by means of the open chain c_2 composed of bodies 5, 6, 1 and flexures A_4 and B_2 . Body 5 is also connected to body 3 by means of the open chain c_3 composed of bodies

Table 3
Geometric parameters of the beam elements.

	Point coordinates		Orientation (rad)
	x (mm)	y (mm)	
Center			Symmetry axis
A ₁	12.73	-90.00	3.14
A ₂	-58.92	-26.67	0.00
A ₃	-46.19	13.93	1.57
A ₄	46.19	-13.93	-1.57
Midpoint			Axis
A ₅	0.00	0.00	0.00
C ₁	46.19	26.67	1.57
C ₂	0.00	53.33	0.79
Vertex			Axis
B ₁	-106.48	-7.37	1.57
B ₂	106.48	7.37	-1.57

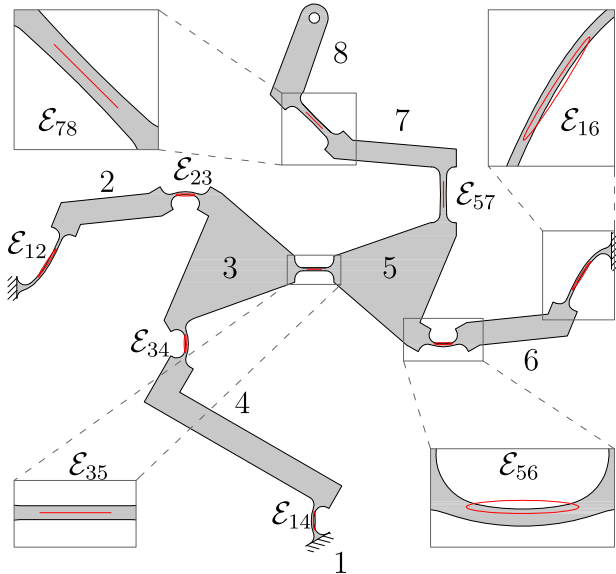


Fig. 8. Ellipses of elasticity relative to the elastic elements.

5, 3, and flexure A₅. Body 3 is connected to the frame 1 by means of two open chains in parallel arrangement. The first one, c₄, is composed of bodies 3, 2, 1, and flexures A₃, B₁. The second one, c₅, is composed of bodies 3, 4, 1, and flexures A₂ and A₁.

The first step consists of the series composition relative to the chains c₁, c₂, c₄, and c₅, that lead to the ellipses \mathcal{E}_{Σ_1} , \mathcal{E}_{Σ_2} , \mathcal{E}_{Σ_4} , and \mathcal{E}_{Σ_5} , respectively. The second step consists of the parallel composition of the ellipses \mathcal{E}_{Σ_4} and \mathcal{E}_{Σ_5} , resulting in \mathcal{E}_{Π_1} , that represents the elastic connection between the body 3 and the frame 1. In the third step, the ellipse \mathcal{E}_{Σ_6} is obtained as series composition of \mathcal{E}_{Π_1} and \mathcal{E}_{35} . In the fourth step, the ellipse \mathcal{E}_{Π_2} is obtained as parallel composition of \mathcal{E}_{Σ_2} and \mathcal{E}_{Σ_6} . The final step consists of the series composition of \mathcal{E}_{Π_2} and \mathcal{E}_{Σ_1} , resulting in \mathcal{E}_{Σ_7} , that represent the compliant mechanism as elastic suspension between body 8 and frame 1. The steps of the procedure are reported in Table 6. The ellipse \mathcal{E}_{Σ_7} is shown in Fig. 9, whereas its parameters are listed in Table 7.

5.3. Kinetostatic analysis

The ellipse of elasticity \mathcal{E}_{Σ_7} establishes a bijective correspondence between the loads applied to the body 8 and its pole of displacements. Therefore, the kinetostatic forward and inverse problems can be solved geometrically exploiting the antiprojective polarity properties. In this case study, according to the finite element simulations and to the experimental campaign reported in Sections 6 and 7, respectively, forces

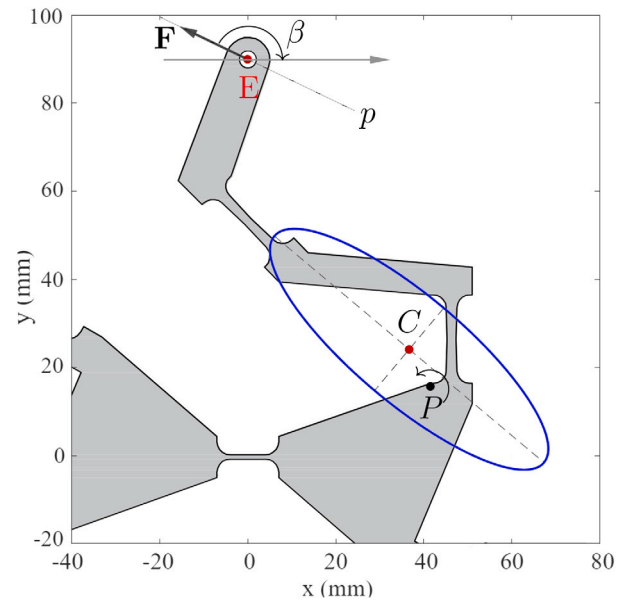


Fig. 9. Ellipse \mathcal{E}_{Σ_7} representing the compliant mechanism as elastic suspension between the end-effector and the frame.

with lines of action passing through E are considered as applied loads and the field of displacements is evaluated for the same point. Given the line of action p, the center of rotation is geometrically determined according to the properties defined in Figs. 3(a)–3(e).

According to Eq. (2), the rotation of the end-effector is given by

$$\theta = w \overline{CE} \times \mathbf{F}. \quad (11)$$

The rotation occurs about P, that is the antipole of p with respect to \mathcal{E}_{Σ_7} (see Fig. 3(d)). Then, the displacement of E can be calculated as

$$\delta = \theta \times \overline{PE}. \quad (12)$$

The theoretical evaluation of the displacements δ consequent to the application of a set of forces \mathbf{F} is reported in Section 8 and compared to the results obtained through finite element analyses and experimental campaign.

6. Finite element analysis

To verify the theoretical results, the kinetostatic analysis of the hybrid compliant mechanism has been also conducted by performing finite element simulations with the commercial software Ansys APDL (www.ansys.com). The mesh, composed of 29757 elements and of 32130 nodes, has been refined in the flexible regions, as shown in Fig. 10. The element PLANE182 has been used in the simulation setup. Fixed supports have been introduced to anchor the model to the fixed frame (points A). The applied load consists of a force with variable magnitude and direction, applied to point E. This load condition is analogous to the one considered in Section 5.3 and Section 7. Two different sets of simulations have been carried out, considering linear deflections and geometric nonlinearities.

7. Experimental test

A polycarbonate monolithic compliant prototype, shown in Fig. 11, has been fabricated by CNC milling process. The material has been characterized through a set of bending tests (Young's modulus $E = 2945$ MPa). The experimental setup, reproducing the load conditions described in Section 5.3, is schematically represented in Fig. 12. The compliant system is anchored to the support with orientation described

Table 4
Geometric and ellipse parameters of the flexible elements.

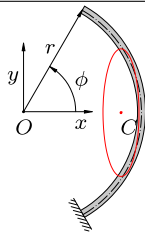
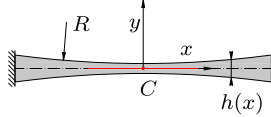
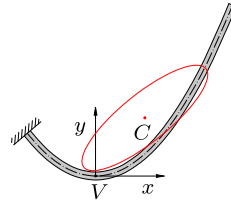
	Uniform, curved	Notched, straight	Uniform, parabolic
			
Geom.	$x = r \cos(\gamma)$ $y = r \sin(\gamma)$ $\gamma \in [-\phi, \phi]$.	$h(x) = h_0 + 2(R - \sqrt{R^2 - x^2})$, $x \in [-l/2, l/2]$.	$y = ax^2$ $x \in [x_1, x_2]$
0th	$w = \frac{2r\phi}{EI}$	$w = \frac{24}{EI} \int_0^{l/2} \frac{dx}{h(x)^3}$	$w = \int_0^l c(s) ds$
1st	$x_C = r \frac{\sin(\phi)}{\phi}$ $y_C = 0$	$x_C = 0$ $y_C = 0$	$x_C = \frac{S_x}{w}$ $y_C = \frac{S_y}{w}$
	$\alpha = 0$	$\alpha = 0$	$\tan 2\alpha = \frac{2S_{x_0y_0}}{S_{y_0y_0} - S_{x_0x_0}}$
2nd	$a^2 = \frac{r^2}{2} \left(1 - \frac{\sin(2\phi)}{2\phi}\right)$ $b^2 = r^2 - (OC^2 + a^2)$	$a^2 = \int_0^{l/2} \frac{x^2}{h(x)^3} dx$ $b^2 = 0$	$a = \sqrt{\frac{S_{xx}}{w}}$ $b = \sqrt{\frac{S_{yy}}{w}}$

Table 5
Parameters of the element ellipses of elasticity: center coordinates (mm), semi-axes lengths (mm), orientations (rad) and elastic weights (rad/mNmm).

\mathcal{E}	x_C	y_C	a	b	α	w
\mathcal{E}_{12}	-95.79	2.01	6.14	0.13	1.00	8.24
\mathcal{E}_{23}	-46.19	26.85	3.30	0.37	0.00	4.47
\mathcal{E}_{34}	-46.01	-26.67	3.30	0.37	1.57	4.47
\mathcal{E}_{14}	-0.18	90.00	3.30	0.37	1.57	4.47
\mathcal{E}_{35}	0.00	0.00	2.60	0.00	0.00	3.47
\mathcal{E}_{36}	46.19	-26.85	3.30	0.37	0.00	4.47
\mathcal{E}_{16}	95.79	-2.01	6.14	0.13	1.00	8.24
\mathcal{E}_{57}	46.19	26.67	4.22	0.00	1.57	0.63
\mathcal{E}_{78}	0.00	53.33	4.22	0.00	2.36	0.63

Table 6
Sequence of serial and parallel compositions of ellipses of elasticity.

Step	Resultant ellipse	Operation	Component ellipses
I	\mathcal{E}_{Σ_1}	Σ	$(\mathcal{E}_{57}, \mathcal{E}_{78})$
	\mathcal{E}_{Σ_2}	Σ	$(\mathcal{E}_{16}, \mathcal{E}_{36})$
	\mathcal{E}_{Σ_3}	Σ	$(\mathcal{E}_{34}, \mathcal{E}_{14})$
	\mathcal{E}_{Σ_4}	Σ	$(\mathcal{E}_{12}, \mathcal{E}_{23})$
II	\mathcal{E}_{Π_1}	Π	$(\mathcal{E}_{\Sigma_1}, \mathcal{E}_{\Sigma_4})$
III	\mathcal{E}_{Σ_5}	Σ	$(\mathcal{E}_{\Pi_1}, \mathcal{E}_{35})$
IV	\mathcal{E}_{Π_2}	Π	$(\mathcal{E}_{\Sigma_5}, \mathcal{E}_{\Sigma_2})$
V	\mathcal{E}_{Σ_7}	Σ	$(\mathcal{E}_{\Pi_2}, \mathcal{E}_{\Sigma_1})$

Table 7
Parameters of the resultant ellipse of elasticity: center coordinates (mm), semi-axes lengths (mm), orientation (rad) and elastic weight (rad/mNmm).

\mathcal{E}	x_C	y_C	a	b	α	w
\mathcal{E}_{Σ_7}	36.69	24.13	39.98	12.23	-0.70	1.78

by the angle β between the global reference frame $R_0 = \{Ox_0y_0\}$ and the local reference frame $R = \{Oxy\}$.

More specifically, R_0 has its origin on the tip E and x -axis parallel to the vertical line. The local reference frame R , attached to the compliant mechanism, is obtained by rotating R_0 , about the z -axis, of the angle β .

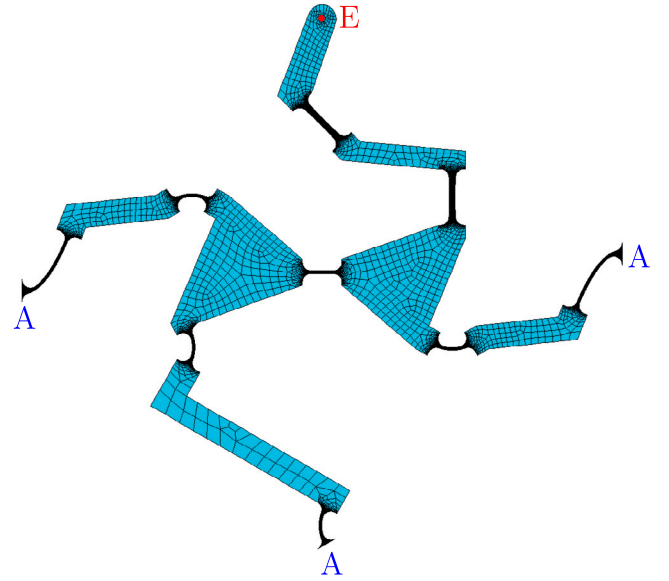


Fig. 10. Generated mesh of the compliant mechanism.

The force is applied to the end-effector by connecting a weight to the tip point E . Several magnitudes and directions have been considered, according to Section 5.3 and Section 6, as detailed in Section 8.

The tip displacements were acquired by using a Logitech Streamcam (www.logitech.com) positioned with the lens plane parallel to the motion plane, as shown in the figure. The displacement analysis was performed by using the video analysis software Tracker 6.1.3 (physlets.org/tracker), as shown in Fig. 13.

8. Results

With reference to Fig. 9, the load condition consists of a set of forces \mathbf{F} with different magnitudes ($F = 0.196, 0.490, 0.981, 1.471$ N) and lines of action p ($\beta = \pi/4, \pi/2, 3\pi/4, \pi$ rad). For each force, the tip

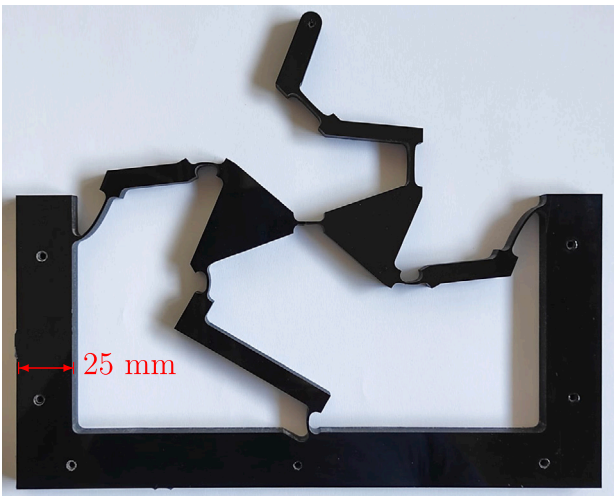


Fig. 11. Polycarbonate sample.

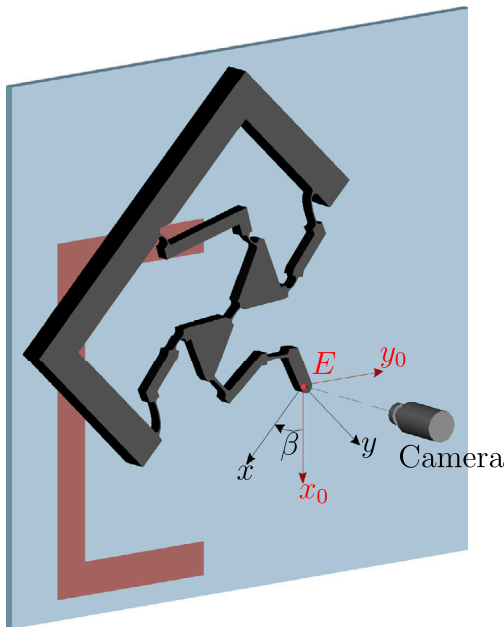


Fig. 12. Schematic of the experimental setup.

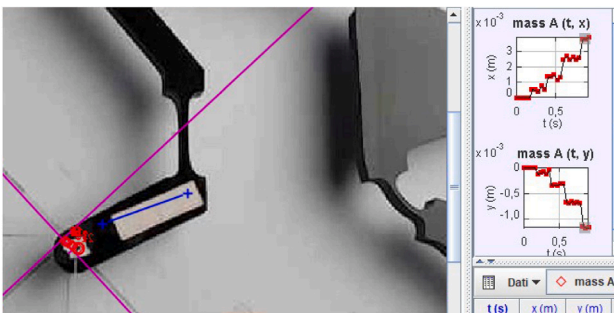


Fig. 13. Tracking of the tip displacements.

displacements are evaluated by resorting to the theoretical model, to the linear and nonlinear FEA, and to the experimental campaign.

The tip displacements, acquired during the test, are first compared to the ones obtained through the theoretical model. The results are

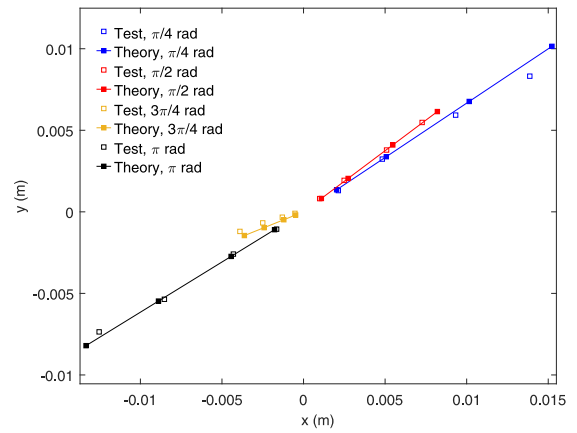


Fig. 14. Theoretical and experimental results: comparison of the tip displacements.

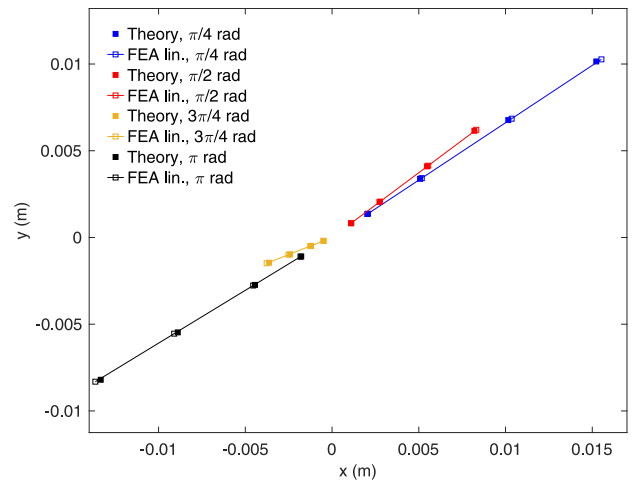


Fig. 15. Comparison of the results obtained by means of theoretical model and linear FEA.

shown in Fig. 14. Generally, the displacement directions and magnitudes are in good agreement. However, for the higher values of the force magnitudes, the theoretical results show greater values of the magnitude displacements. To provide deep insight into these outcomes, linear and nonlinear FEA are included in the comparison.

Firstly, the theoretical displacements are compared to the ones obtained by linear FEA. The results are reported in Fig. 15. In this case, results show very good agreement. The maximum error between theory and FEA, equal to 4.3%, is registered for the force magnitude of 0.981 N at $\pi/2$ rad. Nevertheless, the error mean value, evaluated for all the 16 points, is equal to 2.6%.

A further comparison has been performed between experimental and nonlinear FEA results, depicted in Fig. 16. Some directions, as $3\pi/4$ and π , show greater error with respect to the other ones. This behavior could be ascribed to the fabrication process, or to slight misalignments between the force and the compliant mechanism in the experimental phase. In this case, the medium error is 4.8%.

9. Discussion on distributed compliance

The procedure highlighted in the previous sections results to be particularly suitable for the analysis of compliant mechanisms with lumped compliance. In fact, the ellipse corresponding to each elastic part can be easily defined, determining a straightforward composition of the series and parallel substructures. The same procedure can be applied also to compliant mechanisms with distributed compliance.

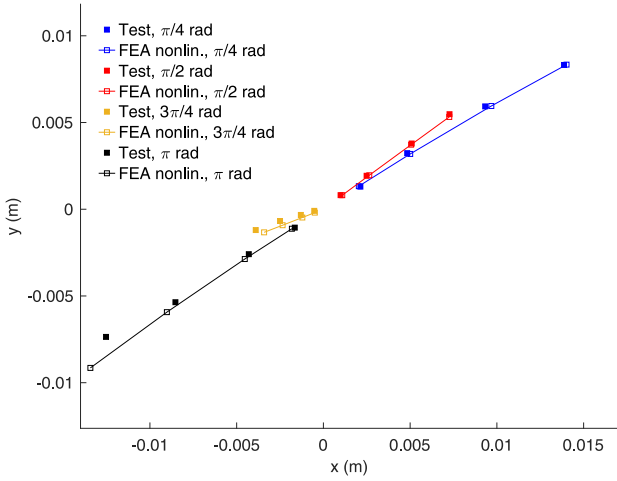


Fig. 16. Comparison of the results obtained by means of experimental test and nonlinear FEA.

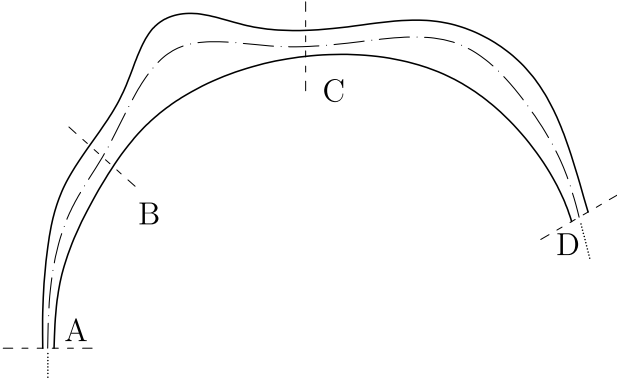


Fig. 17. Generic substructure with distributed compliance.

Fig. 17 shows a generic elastic element, considered as a part of a distributed-compliance mechanism. In this case, different strategies can be adopted, depending on the compliance distribution. For example, the whole element A-D could be considered as a substructure, and the corresponding ellipse determined by solving the zeroth-, first-, and second-order moments of the distribution. A second approach could consist of determining, separately, the ellipses of the parts A-B, B-C, and C-D. Then, the ellipse of A-D could be determined as a series composition of the three elementary ellipses. This strategy could be more efficient of the previous one when the zeroth-, first-, second-order moments of the single parts can be easily solved, numerically or in closed-form, as in the case of elements with constant cross-section or with symmetric axes.

10. Conclusions

In this paper, the theory of the ellipse of elasticity has been applied to the kinetostatic analysis of a compliant mechanism with different flexures and hybrid topology. Uniform flexures with constant and variable curvature, and non-uniform flexures with circular profiles have been considered. From a topological point of view, the compliant mechanism is based on a two-loop Stephenson mechanism, and on a two-link open chain. Firstly, the ellipse of elasticity has been determined at the element level for each flexure. Then, the ellipse at the mechanism level has been obtained by series and parallel compositions. For different load conditions, the kinetostatic analysis has been reduced to the solution of a geometric problem. Finite element simulations

have been performed to ascertain the theoretical results. Furthermore, a polycarbonate monolithic prototype has been fabricated and tested to verify the proposed approach. The mean error values between theoretical approach and linear FEA, and between experimental campaign and nonlinear FEA, resulted to be 2.6% and 4.8%, respectively.

CRedit authorship contribution statement

O. Sorgonà: Writing – review & editing, Writing – original draft, Methodology, Formal analysis, Conceptualization. **S. Serafino:** Writing – review & editing, Validation. **O. Giannini:** Writing – review & editing, Supervision. **M. Verotti:** Writing – original draft, Supervision, Formal analysis, Conceptualization, Writing – review & editing.

Declaration of competing interest

The authors declare that they have no known competing financial interests or personal relationships that could have appeared to influence the work reported in this paper.

Data availability

No data was used for the research described in the article.

Acknowledgments

The authors thank Dr. Gennaro Ponticelli for his support in the fabrication of the monolithic prototype.

Appendix A. Uniform straight beams

Uniform straight beams (joint A_5 in the case study) can be treated as a particular case of constant-curvature beams, with curvature tending to zero. In this case, the center of the ellipse of elasticity coincides with the beam midpoint. In addition, assuming a constant beam length l , and for $\phi \rightarrow 0$, arc equations in Table 4, become

$$w = \frac{l}{EI} \quad (\text{A.1})$$

$$a^2 = l^2 \lim_{\phi \rightarrow 0} \left(\frac{2\phi - \sin(2\phi)}{16\phi^3} \right) = \frac{l^2}{12}, \quad (\text{A.2})$$

$$b^2 = l^2 \lim_{\phi \rightarrow 0} \left(\frac{\phi^2 - \sin(\phi)^2}{4\phi^4} \right) - \frac{l^2}{12} = 0. \quad (\text{A.3})$$

Therefore, the ellipse of elasticity degenerates in a segment having length $2a$, with $a = l\sqrt{3}/6$.

Appendix B. Parabolic arc: zeroth-, first-, second-order moments

The integrals introduced in Section 3.3 result in explicit primitive functions, thanks to the substitution $2ax = \sinh(t)$. Therefore, the generic integrals in the arc-length parameter are transformed as

$$\begin{aligned} \int_0^L f(x(s)) ds &= \int_{x_1}^{x_2} f(x) \sqrt{1 + (2ax)^2} dx \\ &= \frac{1}{2a} \int_{t_1}^{t_2} f\left(\frac{\sinh(t)}{2a}\right) \cosh(t)^2 dt, \end{aligned} \quad (\text{B.1})$$

where $t_1 = \operatorname{arsinh}(2ax_1)$, and $t_2 = \operatorname{arsinh}(2ax_2)$.

The line can be normalized by the transformation of coordinates $\{x, y\} \rightarrow \{u, v\} \equiv \{2ax, 2ay\}$, and the moments can be calculated on the arc

$$v = \frac{1}{2}u^2, \quad u_1 \leq u \leq u_2 : (u_1 = 2ax_1, u_2 = 2ax_2).$$

Moreover, the normalization leads to simpler explicit expressions of the definite integrals. Thus, recalling that

$$\begin{cases} \sinh(t) = u, \\ \cosh(t) = \sqrt{1 + \sinh(t)^2} = \sqrt{1 + u^2}, \\ t = \log(\sinh(t) + \cosh(t)) = \log\left(u + \sqrt{1 + u^2}\right), \end{cases}$$

the moments of the normalized arc read:

$$\begin{aligned} w^* &= 2aw = \frac{1}{EI} \int_{t_1}^{t_2} \cosh(t)^2 dt \\ &= \frac{u(1+u^2)^{1/2} \Big|_{u_1}^{u_2} + \log\left(u + \sqrt{1+u^2}\right) \Big|_{u_1}^{u_2}}{2EI}, \end{aligned} \quad (\text{B.2})$$

$$S_u = 4a^2 S_x = \frac{1}{2EI} \int_{t_1}^{t_2} \sinh(t)^2 \cosh(t)^2 dt = \frac{u(1+u^2)^{3/2} \Big|_{u_1}^{u_2}}{8EI} - \frac{w^*}{8} \quad (\text{B.3})$$

$$S_v = 4a^2 S_y = \frac{1}{EI} \int_{t_1}^{t_2} \sinh(t) \cosh(t)^2 dt = \frac{(1+u^2)^{3/2} \Big|_{u_1}^{u_2}}{3EI}, \quad (\text{B.4})$$

$$\begin{aligned} S_{u_0 u_0} &= 8a^3 S_{x_0 x_0} = S_{uu} - w^* u_c^2 = \\ &= \frac{1}{4EI} \int_{t_1}^{t_2} \sinh(t)^4 \cosh(t)^2 dt - \frac{S_u^2}{w^*} = \frac{u^3(1+u^2)^{3/2} \Big|_{u_1}^{u_2}}{24EI} - \frac{S_u}{4} - \frac{S_u^2}{w^*}, \end{aligned} \quad (\text{B.5})$$

$$\begin{aligned} S_{v_0 v_0} &= 8a^3 S_{y_0 y_0} = S_{vv} - w^* v_c^2 = \frac{1}{EI} \int_{t_1}^{t_2} \sinh(t)^2 \cosh(t)^2 dt - \frac{S_v^2}{w^*} \\ &= 2S_u - \frac{S_v^2}{w^*}, \end{aligned} \quad (\text{B.6})$$

$$\begin{aligned} S_{u_0 v_0} &= 8a^3 S_{x_0 y_0} = S_{uv} - w^* u_c v_c = \\ &= \frac{1}{2EI} \int_{t_1}^{t_2} \sinh(t)^3 \cosh(t)^2 dt - \frac{S_u S_v}{w^*} \\ &= \frac{u^2(1+u^2)^{3/2} \Big|_{u_1}^{u_2}}{10EI} - \frac{S_v}{5} - \frac{S_u S_v}{w^*}, \end{aligned} \quad (\text{B.7})$$

where u_c, v_c are the coordinates of the ellipse center C . In the case $\xi_1 = x_1 = t_1 = 0$, Eqs. (B.2)–(B.7) particularize as

$$w^* = 2aw = \frac{u_2(1+u_2^2)^{1/2} + \log\left(u_2 + \sqrt{1+u_2^2}\right)}{2EI}, \quad (\text{B.8})$$

$$S_u = 4a^2 S_x = \frac{u_2(1+u_2^2)^{3/2}}{8EI} - \frac{w^*}{8}, \quad (\text{B.9})$$

$$S_v = 4a^2 S_y = \frac{(1+u_2^2)^{3/2} - 1}{3EI}, \quad (\text{B.10})$$

$$S_{u_0 u_0} = 8a^3 S_{x_0 x_0} = \frac{u_2^3(1+u_2^2)^{3/2}}{24EI} - \frac{S_u}{4} - \frac{S_u^2}{w^*}, \quad (\text{B.11})$$

$$S_{v_0 v_0} = 8a^3 S_{y_0 y_0} = 2S_x - \frac{S_v^2}{w^*}, \quad (\text{B.12})$$

$$S_{u_0 v_0} = 8a^3 S_{x_0 y_0} = \frac{u_2^2(1+u_2^2)^{3/2}}{10EI} - \frac{S_v}{5} - \frac{S_u S_v}{w^*}. \quad (\text{B.13})$$

Lastly, if $u_1 = -u_2$, it is the arc is symmetric, moments S_y and $S_{x_0 y_0}$ are null, whereas Eqs. (B.8), (B.9), (B.11) and (B.12) hold, provided that the values of the corresponding moments are doubled.

References

Ali, M.A., Shimoda, M., 2023. On multiphysics concurrent multiscale topology optimization for designing porous heat-activated compliant mechanism under convection for additive manufacture. *Eng. Struct.* 294, 116756.

- Arredondo-Soto, M., Cuan-Urquiza, E., Gómez-Espinosa, A., 2022. The compliance matrix method for the kinetostatic analysis of flexure-based compliant parallel mechanisms: Conventions and general force–displacement cases. *Mech. Mach. Theory* 168, 104583.
- Awtar, S., Sen, S., 2010. A generalized constraint model for two-dimensional beam flexures: Nonlinear load-displacement formulation. *J. Mech. Des.* 132 (8).
- Awtar, S., Slocum, A.H., Sevincer, E., 2006. Characteristics of beam-based flexure modules. *J. Mech. Des.* 129 (6), 625–639.
- Balduzzi, G., Aminbaghai, M., Sacco, E., Füssl, J., Eberhardsteiner, J., Auricchio, F., 2016. Non-prismatic beams: A simple and effective timoshenko-like model. *Int. J. Solids Struct.* 90, 236–250.
- Bilancia, P., Baggetta, M., Berselli, G., Bruzzone, L., Fanghella, P., 2021a. Design of a bio-inspired contact-aided compliant wrist. *Robot. Comput.-Integr. Manuf.* 67, 102028.
- Bilancia, P., Baggetta, M., Hao, G., Berselli, G., 2021b. A variable section beams based bi-BCM formulation for the kinetostatic analysis of cross-axis flexural pivots. *Int. J. Mech. Sci.* 205, 106587.
- Bilancia, P., Berselli, G., 2020. Design and testing of a monolithic compliant constant force mechanism. *Smart Mater. Struct.* 29 (4), 044001.
- Bilancia, P., Berselli, G., 2021. An overview of procedures and tools for designing nonstandard beam-based compliant mechanisms. *Comput. Aided Des.* 134, 103001.
- Bodirsky, M., Giménez, O., Kang, M., Noy, M., 2007. Enumeration and limit laws for series-parallel graphs. *European J. Combin.* 28 (8), 2091–2105, *EuroComb '05 - Combinatorics, Graph Theory and Applications*.
- Cammarata, A., Lacagnina, M., Sequenzia, G., 2018. Alternative elliptic integral solution to the beam deflection equations for the design of compliant mechanisms. *Int. J. Interact. Des. Manuf. (IJIDeM)* 13 (2), 499–505.
- Cammarata, A., Sequenzia, G., Oliveri, S.M., Fatuzzo, G., 2016. Modified chain algorithm to study planar compliant mechanisms. *Int. J. Interact. Des. Manuf. (IJIDeM)* 10 (2), 191–201.
- Cao, Z., Yang, R., Guo, H., 2023. Large amplitude free vibration analysis of circular arches with variable thickness. *Eng. Struct.* 294, 116826.
- Chen, G., Liu, X., Gao, H., Jia, J., 2009. A generalized model for conic flexure hinges. *Rev. Sci. Instrum.* 80 (5), 055106.
- Chen, G., Ma, F., Hao, G., Zhu, W., 2019. Modeling large deflections of initially curved beams in compliant mechanisms using chained beam constraint model. *J. Mech. Robotics* 11 (1), 011002.
- Chen, M., Xiao, B., Feng, Y., Yang, T., Zhang, H., Liu, Y., Xu, W., Jiang, H., Wang, Y., 2023. Wave characteristics of reconfigurable elastic metamaterials based on a multi-stable structure. *Eng. Struct.* 280, 115715.
- Chen, W., Zhang, X., Fatikow, S., 2016. Design, modeling and test of a novel compliant orthogonal displacement amplification mechanism for the compact micro-grasping system. *Microsyst. Technol.* 23 (7), 2485–2498.
- Culmann, K., 1875. *Die graphische Statik*. Meyer & Zeller (german).
- Djourachkovitch, T., Blal, N., Hamila, N., Gravouil, A., 2023. Data assisted framework for topology design of micro-architected compliant mechanisms. *Int. J. Solids Struct.* 265–266, 112116.
- Donaldson, B.K., 2008. *Analysis of Aircraft Structures*. Cambridge University Press.
- Dong, W., Chen, F., Gao, F., Yang, M., Sun, L., Du, Z., Tang, J., Zhang, D., 2018. Development and analysis of a bridge-lever-type displacement amplifier based on hybrid flexure hinges. *Precis. Eng.* 54, 171–181.
- Friedrich, R., Lammering, R., Rösner, M., 2014. On the modeling of flexure hinge mechanisms with finite beam elements of variable cross section. *Precis. Eng.* 38 (4), 915–920.
- Glaeser, G., Stachel, H., Odehnal, B., 2016. *The universe of conics*. Springer Spektrum, Berlin, Heidelberg.
- Hao, G., Yu, J., Li, H., 2016. A brief review on nonlinear modeling methods and applications of compliant mechanisms. *Front. Mech. Eng.* 11.
- Hao, G., Zhu, J., 2019. Design of a monolithic double-slider based compliant gripper with large displacement and anti-buckling ability. *Micromachines* 10 (10).
- Howell, L., Magleby, S., Olsen, B., 2013. *Handbook of Compliant Mechanisms*. Wiley.
- Huang, X., Li, Y., Zhou, S., Xie, Y., 2014. Topology optimization of compliant mechanisms with desired structural stiffness. *Eng. Struct.* 79, 13–21.
- Jin, M., Yang, Z., Ynchausti, C., Zhu, B., Zhang, X., Howell, L.L., 2020. Large-deflection analysis of general beams in contact-aided compliant mechanisms using chained pseudo-rigid-body model. *J. Mech. Robotics* 12 (3).
- Kenton, B.J., Leang, K.K., 2012. Design and control of a three-axis serial-kinematic high-bandwidth nanomanipulator. *IEEE/ASME Trans. Mechatronics* 17 (2), 356–369.
- Krishnan, G., Kim, C., Kota, S., 2010. An intrinsic geometric framework for the building block synthesis of single point compliant mechanisms. *J. Mech. Robotics* 3 (1), 011001.
- Kurita, Y., Sugihara, F., Ueda, J., Ogasawara, T., 2012. Piezoelectric tweezer-type end effector with force- and displacement-sensing capability. *IEEE/ASME Trans. Mechatronics* 17 (6), 1039–1048.
- Lang, R.J., Tolman, K.A., Crampton, E.B., Magleby, S.P., Howell, L.L., 2018. A review of thickness-accommodation techniques in origami-inspired engineering. *Appl. Mech. Rev.* 70 (1).
- Li, S., Hao, G., 2022. Design and nonlinear spatial analysis of compliant anti-buckling universal joints. *Int. J. Mech. Sci.* 219, 107111.

- Li, Q., Pan, C., Xu, X., 2013. Closed-form compliance equations for power-function-shaped flexure hinge based on unit-load method. *Precis. Eng.* 37 (1), 135–145.
- Li, P.-Z., Wang, X.-D., Sui, Y.-X., Zhang, D.-F., Wang, D.-F., Dong, L.-J., Ni, M.-Y., 2017. Piezoelectric actuated phase shifter based on external laser interferometer: Design, control and experimental validation. *Sensors* 17 (4), 838.
- Ling, M., Cao, J., Howell, L.L., Zeng, M., 2018. Kinetostatic modeling of complex compliant mechanisms with serial-parallel substructures: A semi-analytical matrix displacement method. *Mech. Mach. Theory* 125, 169–184.
- Ling, M., Cao, J., Jiang, Z., Lin, J., 2016. Theoretical modeling of attenuated displacement amplification for multistage compliant mechanism and its application. *Sensors Actuators A* 249, 15–22.
- Ling, M., Howell, L.L., Cao, J., Chen, G., 2020. Kinetostatic and dynamic modeling of flexure-based compliant mechanisms: A survey. *Appl. Mech. Rev.* 72 (3), 030802.
- Lipkin, H., Patterson, T., 1992a. Geometrical properties of modelled robot elasticity: Part I — decomposition. In: 22nd Biennial Mechanisms Conference: Robotics, Spatial Mechanisms, and Mechanical Systems. American Society of Mechanical Engineers, pp. 179–185.
- Lipkin, H., Patterson, T., 1992b. Geometrical properties of modelled robot elasticity: Part II — center of elasticity. In: 22nd Biennial Mechanisms Conference: Robotics, Spatial Mechanisms, and Mechanical Systems. American Society of Mechanical Engineers, pp. 187–193.
- Lobontiu, N., 2014. Compliance-based matrix method for modeling the quasi-static response of planar serial flexure-hinge mechanisms. *Precis. Eng.* 38 (3), 639–650.
- Lobontiu, N., Paine, J.S.N., Garcia, E., Goldfarb, M., 2000. Corner-filleted flexure hinges. *J. Mech. Des.* 123 (3), 346–352.
- Lobontiu, N., Paine, J.S., O'Malley, E., Samuelson, M., 2002. Parabolic and hyperbolic flexure hinges: flexibility, motion precision and stress characterization based on compliance closed-form equations. *Precis. Eng.* 26 (2), 183–192.
- Luo, Y., Liu, W., Wu, L., 2015. Analysis of the displacement of lumped compliant parallel-guiding mechanism considering parasitic rotation and deflection on the guiding plate and rigid beams. *Mech. Mach. Theory* 91, 50–68.
- Morales Bieze, T., Kruszewski, A., Carrez, B., Duriez, C., 2020. Design, implementation, and control of a deformable manipulator robot based on a compliant spine. *Int. J. Robot. Res.* 39 (14), 1604–1619.
- Qu, J., Chen, W., Zhang, J., Chen, W., 2016. A piezo-driven 2-DOF compliant micropositioning stage with remote center of motion. *Sensors Actuators A* 239, 114–126.
- Radaelli, G., Herder, J., 2017. Gravity balanced compliant shell mechanisms. *Int. J. Solids Struct.* 118–119, 78–88.
- Ritter, W., 1888. *Anwendungen der graphischen statik*, vol. 1, Meyer & Zeller (german).
- Saito, K., Iwata, K., Ishihara, Y., Sugita, K., Takato, M., Uchikoba, F., 2016. Miniaturized rotary actuators using shape memory alloy for insect-type MEMS microrobot. *Micromachines* 7 (4).
- Santer, M., Pellegrino, S., 2008. Compliant multistable structural elements. *Int. J. Solids Struct.* 45 (24), 6190–6204.
- Schultz, J., Ueda, J., 2013. Two-port network models for compliant rhomboidal strain amplifiers. *IEEE Trans. Robotics* 29 (1), 42–54.
- Shooshitari, A., Khajavi, R., 2010. An efficient procedure to find shape functions and stiffness matrices of nonprismatic Euler–Bernoulli and timoshenko beam elements. *Eur. J. Mech. A Solids* 29 (5), 826–836.
- Sorgonà, O., Belfiore, N., Giannini, O., Verotti, M., 2023. Application of the ellipse of elasticity theory to the functional analysis of planar compliant mechanisms. *Mech. Mach. Theory* 184, 105308.
- Su, H.-J., Shi, H., Yu, J., 2012. A symbolic formulation for analytical compliance analysis and synthesis of flexure mechanisms. *J. Mech. Des.* 134 (5).
- Tsai, L., 2000. *Mechanism design: Enumeration of kinematic structures according to function*. Mechanical and Aerospace Engineering Series, CRC Press.
- Ueda, J., Secord, T.W., Asada, H.H., 2010. Large effective-strain piezoelectric actuators using nested cellular architecture with exponential strain amplification mechanisms. *IEEE/ASME Trans. Mechatronics* 15 (5), 770–782.
- Verotti, M., Dochshanov, A., Belfiore, N.P., 2017. A comprehensive survey on microgrippers design: Mechanical structure. *J. Mech. Des.* 139 (6).
- Wang, T., Li, Y., Zhang, Y., Lin, R., Qian, J., Dou, Z., 2021. Design of a flexure-based parallel XY micropositioning stage with millimeter workspace and high bandwidth. *Sensors Actuators A* 112899.
- Wang, P., Xu, Q., 2018. Design and modeling of constant-force mechanisms: A survey. *Mech. Mach. Theory* 119, 1–21.
- Wu, S., Shao, Z., Fu, H., 2022. A substructure condensed approach for kinetostatic modeling of compliant mechanisms with complex topology. *Micromachines* 13 (10), 1734.
- Wu, S., Shao, Z., Su, H., Fu, H., 2019. An energy-based approach for kinetostatic modeling of general compliant mechanisms. *Mech. Mach. Theory* 142, 103588.
- Wu, Z., Xu, Q., 2018. Survey on recent designs of compliant micro-/nano-positioning stages. *Actuators* 7 (1), 5.
- Xu, Q., Li, Y., 2011. Analytical modeling, optimization and testing of a compound bridge-type compliant displacement amplifier. *Mech. Mach. Theory* 46 (2), 183–200.
- Yong, Y.K., Mohemani, S.O.R., 2013. Design of an inertially counterbalanced z -nanopositioner for high-speed atomic force microscopy. *IEEE Trans. Nanotechnol.* 12 (2), 137–145.
- Zhang, A., Chen, G., 2013. A comprehensive elliptic integral solution to the large deflection problems of thin beams in compliant mechanisms. *J. Mech. Robotics* 5 (2).
- Zhao, L., Yu, X., Li, P., Qiao, Y., 2020. High-precision compliant mechanism for lens XY micro-adjustment. *Rev. Sci. Instrum.* 91 (3), 035004.
- Zhu, Z., To, S., Zhu, W.-L., Li, Y., Huang, P., 2018a. Optimum design of a piezo-actuated triaxial compliant mechanism for nanocutting. *IEEE Trans. Ind. Electron.* 65 (8), 6362–6371.
- Zhu, W.-L., Zhu, Z., Guo, P., Ju, B.-F., 2018b. A novel hybrid actuation mechanism based XY nanopositioning stage with totally decoupled kinematics. *Mech. Syst. Signal Process.* 99, 747–759.